STRUCTURAL CONTROL AND HEALTH MONITORING
Struct. Control Health Monit. (2010)
Published online in Wiley InterScience (www.interscience.wiley.com). DOI: 10.1002/stc.395

Fatigue predictions in entire body of metallic structures from a limited number of vibration sensors using Kalman filtering

Costas Papadimitriou[1,*,†], Claus-Peter Fritzen[2], Peter Kraemer[2] and Evangelos Ntotsios[1]

[1]*Department of Mechanical Engineering, University of Thessaly, Volos 38334, Greece*
[2]*Institute of Mechanics and Control Engineering, University of Siegen, Siegen 57076, Germany*

SUMMARY

A methodology is proposed for estimating damage accumulation due to fatigue in the entire body of a metallic structure using output-only vibration measurements from a sensor network installed at a limited number of structural locations. Available frequency domain stochastic fatigue methods based on Palmgren-Miner damage rule, S-N fatigue curves on simple specimens subjected to constant amplitude loads, and Dirlik's probability distribution of the stress range are used to predict the expected fatigue damage accumulation of the structure in terms of the power spectral density (PSD) of the stress processes. The PSD of stresses at unmeasured locations are estimated from the response time history measurements available at the limited measured locations using Kalman filter and a dynamic model of the structure. The effectiveness and accuracy of the proposed formulation is demonstrated using a multidegree-of-freedom spring-mass chain model and a two-dimensional truss model arising from structures that consist of members with uniaxial stress states. Copyright © 2010 John Wiley & Sons, Ltd.

Received 27 October 2009; Revised 5 March 2010; Accepted 25 March 2010

KEY WORDS: life prediction; stochastic fatigue; dynamic analysis; spectral methods; Kalman filter

1. INTRODUCTION

Damage accumulation due to fatigue is an important safety-related issue in metallic structures. The linear Palmgren-Miner damage accumulation law [1,2] is often used to evaluate fatigue damage using available methods for cycle counting in variable amplitude measured stress response time histories and S-N curves obtained from laboratory experiments of simple specimens subjected to constant amplitude loads. The damage accumulation predictions are based on time histories measurements taken from a sensor network, consisting usually of strain rosettes, attached to the structure. Such predictions are only applicable for the locations where measurements are available. Due to practical and economical considerations, the number of sensors placed in a structure during operation is very limited and in most cases they do not cover all critical locations. Moreover, there are locations in the structure that one cannot install

*Correspondence to: Costas Papadimitriou, Department of Mechanical Engineering, University of Thessaly, Volos 38334, Greece.
†E-mail: costasp@uth.gr

Contract/grant sponsor: Greek National Scholarship Foundation (IKY)
Contract/grant sponsor: Deutscher Akademischer Austausch Dienst
Contract/grant sponsor: Greek Ministry of Development (General Secretariat of Research and Technology)
Contract/grant sponsor: European Social Fund

sensors, such as submerged structures, underwater locations in offshore structures (oil refinery structures, offshore wind turbines, offshore steel jackets, etc.), heated structural components, internal points in solid structures, and non-approachable areas of large extended structures. Available fatigue prediction methods based only on measurements cannot be used to predict fatigue damage accumulation at such locations where measurements are not available. To infer damage due to fatigue at structural members where measurements are not available, one needs to predict the stress response time histories in these structural members using the available measurements obtained from the sensory system. In certain circumstances, such predictions can be possible if one combines the available measurements with the information obtained from a dynamic model (e.g. a finite element model) of the structure.

The methods for fatigue damage accumulation have been extended to treat the case that the excitations can be represented by a stochastic vector process with known correlation characteristics. Assuming that the structure behaves linearly and the excitation is modeled by a Gaussian stochastic vector process, the stress response at any point is a stochastic process that can be completely defined using the correlation characteristics of the stochastic excitations [3]. The fatigue damage accumulation at a structural location can then be computed using the characteristics of the stochastic processes of the components of the stress tensor at such a location. Methods for fatigue damage accumulation for Gaussian narrow-band stress processes have been introduced using the Rayleigh approximation and extended to handle the case of wide-band Gaussian stress processes (e.g. [4–16]). Reviews and comparisons of selected spectral methods for stochastic fatigue analysis based on wide-band Gaussian stochastic processes can be found in Benasciutti and Tovo [9] and Larsen and Lutes [12]. The formulations depend on the probability distribution of stress cycles corresponding to different stress levels in a stress response time history signal and the expected number of peaks per unit time of a stress process. Results for the expected fatigue damage accumulation predicted by the Palmgren-Miner linear law have been presented in terms of the spectral moments of the stress process which are readily obtained from the power spectral density (PSD) of the stress components involved. For the important case of wide-band processes encountered often in applications, the simulation-inspired Dirlik approximation [8] is widely used and is considered to be the most accurate formula for modeling the probability of stress cycles in terms of the spectral moments of the stress process. It is worth noting that the aforementioned frequency domain methods based on the stress power spectral densities or spectral moments use no information available from a sensor network. Instead, their predictive accuracy depends on the assumptions employed for the excitation characteristics and the models representing the structural behavior. However, these predictions fail to integrate the information provided by a network of sensors. The sensor information is expected to update and improve the fatigue predictions, making them consistent with the available measurements.

This study addresses the problem of estimating the expected damage accumulation or remaining lifetime due to fatigue in the entire body of a structure using output-only vibration measurements at a limited number of locations provided by a sensor network installed on the structure. The measurements may consist of response time histories, such as e.g., strain, acceleration, velocity, displacement, etc. The expected fatigue damage accumulation in the entire structure is obtained by integrating (a) methods for predicting strain/stress response time histories and their correlation/spectral characteristics in the entire structure from output-only measured response time histories available at limited locations in the structure, and (b) frequency domain methods for estimating fatigue damage accumulation using the spectral characteristics of the predicted strain/stress response time histories. The idea is to use Kalman filter (KF) [17] methods to predict the strain/stress response time histories at various locations within structural components using the measurements available at a limited number of locations. A schematic diagram of the fatigue lifetime prediction in the entire structure from limited number of sensors using KF, along with its use in inspection/maintenance decisions, is shown in Figure 1. Response time history measurements are collected from a limited number of points $S_1, \ldots, S_n$, whereas stress time history predictions are made at any number of points $P_1, \ldots, P_m$. For each prediction point P, the fatigue damage accumulation, or remaining fatigue

DOI: 10.1002/stc

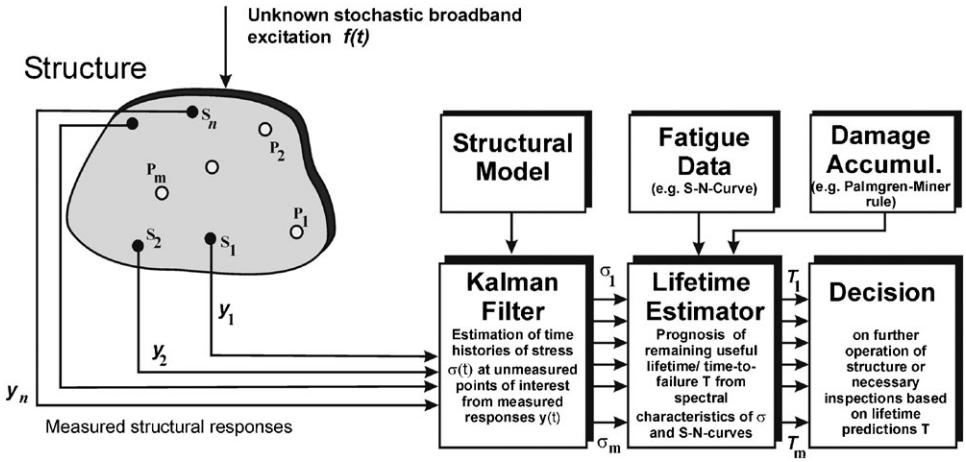

Figure 1. Scheme of lifetime prediction from a limited number of sensors using a KF.

lifetime T, is obtained by combining the information in the stress tensor time history $\sigma(t)$ for the point P, fatigue data sets (e.g. S-N-curves) and a damage accumulation model (e.g. Palmgren-Miner rule). Such predictions are restricted in this study to the case of linear structures and excitations that can be adequately represented by Gaussian stationary stochastic processes. The excitation time histories applied in the structure are considered to be unknown. However, for several operational conditions of structures, the excitation time histories can be considered to be samples of a Gaussian stationary stochastic process with unknown intensity and frequency content. The proposed methodology is thus applicable for the case where the responses can be modeled by Gaussian stationary processes and the measured response time histories are long enough so that they can be considered to be samples of stationary processes.

The objective of this study is to formulate the fatigue prediction problem, illustrate the methodology, and point out its use in evaluating the damage accumulation in the entire structure from a limited number of vibration measurements. For this, the present approach is limited to uniaxial stress processes and simplified models of structures. The extension to multiaxial stress processes can be accomplished by using recent developments in frequency domain methods for stochastic fatigue based on spectral techniques [18–20]. These methods reduce the multiaxial stress state to an equivalent uniaxial stress state that can be treated by available fatigue estimation techniques based on spectral methods. In addition, extension to non-Gaussian stress processes, known to significantly affect fatigue life predictions [5,21], can also be accomplished by using recent approximations for the probability distribution of the stress cycles [22] in terms also of the higher moments of the stress process, such as skewness and kurtosis. In addition, the proposed method could be extended to handle fracture mechanics approaches to random fatigue [23], such as stochastic fatigue crack growth problems [24,25], provided that governing equations for damage evolution are conveniently described with respect to the PSD or its spectral moments of the stress process at a point [26].

This study is organized as follows. In Section 2, the frequency domain formulation for predicting damage due to fatigue in structural elements subjected to uniaxial stress state in linear structures under Gaussian stochastic excitations is reviewed. The formulation is applicable to Gaussian wide-band stress processes, often encountered in engineering applications, and damage accumulation due to fatigue depends on the spectral moments of the power spectral densities of the stress process at a location of a structure. Section 3 presents the formulation for predicting the strain/stress response time histories and the associated power spectral densities at all desirable locations of the structure using the KF and the measured time histories at a limited number of locations in the structure. For this, the state space formulation of the equations governing the vibrations of a structure is briefly summarized in Section 3.1. Using the discrete-time formulation of the state space approach, the KF approach for estimating the power spectral densities of the stresses in the entire body of the structure is presented in

DOI: 10.1002/stc

Section 3.2 and 3.3. The approach considers that the unmeasured excitations can be represented by Gaussian stationary stochastic processes. Finally, Section 4 demonstrates the effectiveness of the proposed methodology using a chain-like mass-spring multidegree-of-freedom structure and 'measured' data that are simulated from various types of excitations, including white noise and filtered white noise excitations. Conclusions are summarized in Section 5.

2. FREQUENCY DOMAIN METHOD FOR FATIGUE ESTIMATION BASED ON SPECTRAL MOMENTS

The Palmgren-Miner rule [1,2] is commonly used to predict the damage accumulation due to fatigue. According to this rule, a linear damage accumulation law at a point in the structure subjected to variable amplitude stress time history is defined by the formula

$$D = \sum_{i}^{m} \frac{n_i}{N_i} \tag{1}$$

where n_i is the number of cycles at a stress level σ_i, N_i is the number of cycles required for failure at a stress level σ_i, and m is the number of stress levels identified in a stress time history at the corresponding structural point. Available S-N fatigue curves, obtained from laboratory experiments on simple specimens that are subjected to constant amplitude loads, are used to describe the number of cycles N_i required for failure in terms of the stress level σ_i. The number of cycles n_i at a stress level σ_i are usually obtained using available stress cycle counting methods, provided that the stress time histories are available through measurements. Alternatively, for the cases where the stress response time histories are not available from measurements, frequency domain methods based on spectral moments (e.g. [5,9]) can be used to predict the expected damage due to fatigue using the linear damage law (1). The methodology assumes that the PSD of the stress process at a structural location is available. For linear systems excited by time-varying loads that can be modeled by stationary stochastic processes, these power spectral densities can be straightforwardly computed using available random vibration results [3].

The following section outlines such a frequency domain methodology based on spectral moments for fatigue estimation for structural members subjected to uniaxial stress state. For multiaxial stress states, one can apply available methods [18–20] to extend the applicability of the present methodology. Let $\sigma(t)$ be the uniaxial stress at a point in a structural element. The stress is considered to be a stationary Gaussian stochastic process. This is the case encountered in linear structures that are subjected to stationary Gaussian stochastic processes. Let $S_\sigma(\omega)$ be the PSD of the stationary Gaussian stochastic stress process $\sigma(t)$ of the uniaxial stress at a structural location and

$$\lambda_j = \int_{-\infty}^{\infty} |\omega|^j S_\sigma(\omega)\, \mathrm{d}\omega \tag{2}$$

be the spectral moments of the process. Using frequency domain methods for fatigue estimation under stochastic excitations and the continuous version of the damage accumulation law (1), the expected fatigue damage accumulation for a uniaxial stochastic stress process is given by [9]

$$E[D] = \int_0^{\infty} \frac{n(\sigma)}{N(\sigma)} \mathrm{d}\sigma = c^{-1} T\, E[P] \int_0^{\infty} \sigma^{\alpha} p(\sigma)\, \mathrm{d}\sigma \tag{3}$$

where $n(\sigma) = T\, E[P] p(\sigma)\, \mathrm{d}\sigma$ is the number of cycles at stress levels within the stress interval $[\sigma, \sigma + \mathrm{d}\sigma]$, $p(\sigma)$ is the probability distribution of the stress levels,

$$N(\sigma) = c\sigma^{-\alpha} \tag{4}$$

is the number of cycles for failure that correspond to a specific constant amplitude stress level σ obtained from available S-N curves, $E[P]$ is the expected number of peaks per unit time for the stress process, and T the period of observation. The parameters c and α are constants obtained from fatigue test experiments and depend on the material and the type of the test specimen.

DOI: 10.1002/stc

The expected time of failure due to fatigue (fatigue lifetime) T_{life} corresponds to a critical expected damage value $E[D] = D_{\text{cr}}$ which is often set equal to unity ($D_{\text{cr}} = 1$). Using Equation (3), the fatigue lifetime is given by

$$T_{\text{life}} = \frac{D_{\text{cr}}}{\bar{D}} \tag{5}$$

where $\bar{D}$ is the expected damage rate given by

$$\bar{D} = c^{-1} E[P] \int_0^\infty \sigma^\alpha p(\sigma)\, \mathrm{d}\sigma \tag{6}$$

For Gaussian stochastic stress processes, the probability distribution of the stress range $\Delta\sigma = 2\sigma$, taken to be twice the random amplitude at stress level within $[\sigma,\sigma+\mathrm{d}\sigma]$ in a stress process, is given by the Dirlik formula [8,27,28] as

$$p(\Delta\sigma) = \frac{1}{2\sqrt{\lambda_0}} \left[\frac{d_1}{h} e^{-\frac{\Delta\sigma}{2h\sqrt{\lambda_0}}} + \frac{d_2 \Delta\sigma}{2r^2\sqrt{\lambda_0}} e^{-\frac{(\Delta\sigma)^2}{8r^2\lambda_0}} + \frac{d_3 \Delta\sigma}{2\sqrt{\lambda_0}} e^{-\frac{(\Delta\sigma)^2}{8\lambda_0}} \right] \tag{7}$$

where d_1, d_2, d_3, h and r are specific algebraic functions of the spectral moments λ_0, λ_1, λ_2, and λ_4, given by

$$d_1 = \frac{2(x_m - \alpha_2^2)}{1+\alpha_2^2}, \quad d_2 = \frac{1 - \alpha_2 - d_1 + d_1^2}{1 - r}, \quad d_3 = 1 - d_1 - d_2 \tag{8}$$

$$h = \frac{1.25(\alpha_2 - d_3 - d_2 r)}{d_1}, \quad r = \frac{\alpha_2 - x_m - d_1^2}{1 - \alpha_2 - d_1 + d_1^2} \tag{9}$$

$$x_m = \frac{\lambda_1}{\lambda_0} \left[\frac{\lambda_2}{\lambda_4} \right]^{\frac{1}{2}} = \alpha_1 \alpha_2, \quad \alpha_1 = \frac{\lambda_1}{\sqrt{\lambda_0 \lambda_2}}, \quad \alpha_2 = \frac{\lambda_2}{\sqrt{\lambda_0 \lambda_4}} \tag{10}$$

This is a semi-empirical probability density, which is a mixture of one exponential and two Rayleigh distributions. It has been derived by fitting the shape of a rainflow range distribution via minimizing the normalized error between the rainflow ranges and the above density model. The spectral moments λ_0, λ_1, λ_2, and λ_4 constitute a base for the construction of the approximate closed-form Dirlik formula for the probability density of the stress range. The Dirlik formula constitutes an extension of the Rayleigh distribution to non-narrow band processes. It is widely used for fatigue estimation under wide-band Gaussian stationary applied stress. Extension to non-Gaussian stress processes requiring the skewness and kurtosis of the stress process are available in the work by Wang and Sun [22].

Using results from random vibration theory, the expected number of cycles $E[P]$ per second for a stochastic process is given by the spectral moments of the process in the form

$$E[P] = \frac{1}{2\pi} \sqrt{\frac{\lambda_4}{\lambda_2}} \tag{11}$$

Starting with (6) and noting that $p(\sigma) = p(\Delta\sigma)/2 = p(2\sigma)/2$, then substituting (11) and the Dirlik formula (7) into (6) and finally carrying out the integration in (6) analytically, the expected damage rate simplifies to [9]

$$\bar{D} = (8\pi c)^{-1} \sqrt{\frac{\lambda_4}{\lambda_2}} \lambda_0^{\alpha/2} \left[d_1 h^\alpha \Gamma(1+\alpha) + 2^{\alpha/2} \Gamma\left(1 + \frac{\alpha}{2}\right) (d_2 |r|^a + d_3) \right] \tag{12}$$

where d_1, d_2, d_3, h and r are defined in (8)–(10).

It is clear from the aforementioned formulation and equations (5) and (12) that the expected fatigue damage rate $\bar{D}$ and, consequently, the fatigue accumulation during a time interval T or the fatigue lifetime T_{life} at a point in the structure depends only on the spectral moments λ_i, $i = 0,1,2,4$, of the stress process $\sigma(t)$. Using the definition of the spectral moments in (2), the spectral moments and the fatigue predictions at a point of a structure eventually depend only on the PSD $S_\sigma(\omega)$ of the stress process $\sigma(t)$. It should be noted that the fatigue damage rate in (12) is

DOI: 10.1002/stc

based on Dirlik's approximation for the probability distribution of the stress ranges. In the literature, several spectral-based approximations [4–7,9–16] have been proposed to compute fatigue lifetime in terms of the spectral moments of the stress process. These methods can also be used as alternatives to Dirlik's approximation to compute fatigue. The fatigue lifetime estimates will depend on the method used. In this study, the approximation (12) is chosen as one of the several alternative approximations to illustrate the method proposed for fatigue predictions at unmeasured locations.

The power spectral densities of the stress response processes at a point can be calculated from measurements. However, there is a limited number of points that can be instrumented in the structure. For the points where measurements are not available, one has to make predictions of the stress process and subsequently the PSD of the stress process at a location, given the measurements at other locations. This issue of predicting the power spectral densities of the stress processes in the entire body of the structure using measurements at limited locations is addressed at the next Section 3. Once these measurements and predictions of the stresses are estimated at measured and unmeasured locations, the power spectral densities and the corresponding damage accumulation or lifetime due to fatigue are obtained, using (5) and (12), everywhere in the structure. In this way, fatigue damage accumulation maps for the entire structure are constructed from the limited number of ambient vibration measurements.

3. RESPONSE PREDICTIONS IN THE ENTIRE STRUCTURE USING AMBIENT VIBRATION MEASUREMENTS

The objective of this section is to predict the stress response at all points in a structure using the measurements at a limited number of locations. This is achieved using an approach that is outlined in the next two subsections based on the commonly used KF method [17] for full state estimation of a linear system using limited number of measurements.

3.1. Equations of motion and state space formulation

Consider the dynamic response of a linear structural system subjected to deterministic and random excitations. Using a spatial discretization method, such as finite element analysis, the equations of motion are given by the following set of N second-order differential equations

$$M\underline{\ddot{q}}(t)+C\underline{\dot{q}}(t)+K\underline{q}(t) = L_u\underline{u}(t)+L_w\underline{w}(t) \tag{13}$$

where $\underline{q}(t) \in \mathbb{R}^{N\times 1}$ is the displacement vector, M, C and $K \in \mathbb{R}^{N\times N}$ are the mass, damping and stiffness matrices, respectively, $\underline{u}(t) \in \mathbb{R}^{N_{u,in}\times 1}$ and $\underline{w}(t) \in \mathbb{R}^{N_{w,in}\times 1}$ are the applied deterministic and stochastic excitation vectors of dimension $N_{u,\mathrm{in}}$ and $N_{w,\mathrm{in}}$, respectively, and $L_u \in \mathbb{R}^{N\times N_{u,\mathrm{in}}}$ and $L_w \in \mathbb{R}^{N\times N_{w,\mathrm{in}}}$ are matrices comprised of zeros and ones that map the $N_{u,\mathrm{in}}$ and $N_{w,\mathrm{in}}$ deterministic and stochastic excitation loads to the N output DOFs. Throughout the analysis, it is assumed that the system matrices M, C and K are symmetric. Let $\underline{y}(t) \in \mathbb{R}^{N_{\mathrm{meas}}}$ be the vector that collects all measurements at different locations of the structure at time t. These measurements are generally collected from sensors, such as accelerometers, strain gauges, etc. For convenience and without loss of generality, it is assumed in the analysis that sensors placed in the structure measure the strains.

Introducing the state vector $\underline{x}^{\mathrm{T}} = [\underline{q}^{\mathrm{T}} \;\; \underline{\dot{q}}^{\mathrm{T}}] \in \mathbb{R}^{1\times 2N}$, the equation of motion can be written in the state space form

$$\underline{\dot{x}} = A_c\underline{x}+B_c\underline{u}(t)+G_c\underline{w}(t) \tag{14}$$

while the measured output vector $\underline{y}(t)$ is given by the observation equation

$$\underline{y}(t) = H\underline{x}+D\underline{u}(t) \tag{15}$$

DOI: 10.1002/stc

where the state transition matrix A_c, and the matrices B_c and G_c are given by

$$A_c = \begin{bmatrix} 0 & I \\ -M^{-1}K & -M^{-1}C \end{bmatrix} \in \mathbb{R}^{2N\times 2N} \tag{16}$$

$$B_c = \begin{bmatrix} 0 \\ -M^{-1}L_u \end{bmatrix} \in \mathbb{R}^{2N\times N_{u,\text{in}}} \quad \text{and} \quad G_c = \begin{bmatrix} 0 \\ -M^{-1}L_w \end{bmatrix} \in \mathbb{R}^{2N\times N_{w,\text{in}}} \tag{17}$$

respectively, $H \in \mathbb{R}^{N_{\text{meas}}\times 2N}$ is the observation matrix and $D = 0 \in \mathbb{R}^{N_{\text{meas}}\times 2N_{u,in}}$ for strain measurements.

3.2. Kalman filter approach

As measurements are available in digitized form, the presentation of the KF is next given in discrete time. Using the sampling rate $1/\Delta t$, the discrete-time state space model corresponding to (14) and (15) is

$$\underline{x}_k = A\underline{x}_{k-1} + B\underline{u}_{k-1} + G\underline{w}_{k-1} \tag{18}$$

$$\underline{y}_k = H\underline{x}_k + D\underline{u}_k + \underline{v}_k \tag{19}$$

where $\underline{x}_k = \underline{x}(k\Delta t)$ and $\underline{y}_k = \underline{y}(k\Delta t)$, $k = 1, \ldots, N_s$, are the digitized state and output vectors, $A = e^{A_c\Delta t}$ is the state transition matrix for the discrete formulation, B and G are the matrices arising from B_c and G_c after converting the state space model (14) from continuous to discrete time. The random variables w_k and v_k represent the stochastic excitation and the measurement noise, respectively. They are assumed to be independent, white and following normal probability distributions $p(w_k) \sim N(0, Q)$ and $p(v_k) \sim N(0, R)$, where Q and R are the stochastic excitation and the measurement noise covariances assumed to be constant, independent of time.

KF is used to estimate the state $\hat{\underline{x}}_k$ of the system described by (18) using the measurements in the vector $\underline{y}_k$ in (19). Specifically, in the prediction step, an apriori state estimate $\hat{\underline{x}}_k^-$ of the state vector $\underline{x}_k$ of the system is estimated from equation [29,30]

$$\hat{\underline{x}}_k^- = A\hat{\underline{x}}_{k-1} + B\underline{u}_{k-1} \tag{20}$$

In the correction step, the measured value $\underline{y}_k$ is used to calculate a posteriori state estimate $\hat{\underline{x}}_k$, weighting the measured and estimated signals by the KF gain factor K_k. This is formulated by the equation

$$\hat{\underline{x}}_k = \hat{\underline{x}}_k^- + K_k[\underline{y}_k - H\hat{\underline{x}}_k^- - D\underline{u}_k] \tag{21}$$

where the Kalman gain factor is given by

$$K_k = P_k H^{\mathrm{T}}[HP_k H^{\mathrm{T}} + R]^{-1} \tag{22}$$

and, for steady state response, the error covariance matrix $P_k \equiv P = E[\underline{e}_k^-(\underline{e}_k^-)^{\mathrm{T}}]$, where $\underline{e}_k^- = \underline{x} - \hat{\underline{x}}_k^-$ is the a priori error estimate, satisfies the discrete time Riccati equation:

$$P = APA^{\mathrm{T}} - APH^{\mathrm{T}}(HPH^{\mathrm{T}} + R)^{-1}HPA^{\mathrm{T}} + GQG^{\mathrm{T}} \tag{23}$$

Let $\underline{\sigma}_k$ be a vector containing the digitized stresses at time $t = k\Delta t$ at various locations of the structure. Using structural mechanics theory, these stresses in the vector $\underline{\sigma}_k$ are related to the state vector through a linear transformation $\underline{\sigma}_k = \Sigma\underline{x}_k$, where Σ is the transformation matrix that associates the state vector to the desired stresses in the entire structure. Consequently, an estimate of the stresses $\hat{\underline{\sigma}}_k$ is related to the state vector estimate $\hat{\underline{x}}_k$ through the transformation:

$$\hat{\underline{\sigma}}_k = \Sigma\hat{\underline{x}}_k \tag{24}$$

In this study, the response prediction vector $\underline{\sigma}_k$ is restricted to stresses at elements subjected to uniaxial stress states required in lifetime fatigue estimation as described in Section 2.

Using the definition of the cross PSD (CPSD), the KF equations (20) and (21), the fact that $B = 0$ in (20) for the case of stochastic excitations and $D = 0$ in (21) for strain measurements, the CPSD $S_{\hat{\underline{\sigma}}}(\omega)$ of the stress response vector $\hat{\underline{\sigma}}_k$ can readily be obtained with respect to the CPSD

DOI: 10.1002/stc

$S_{\underline{y}}(\omega)$ of the measurement vector $\underline{y}_k$ in the form

$$S_{\underline{\hat{\sigma}}}(\omega) = \Sigma S_{\underline{x}}(\omega)\Sigma^{\mathrm{T}} = \Sigma\, Z^{-1}(j\omega)KS_{\underline{y}}(\omega)K^{\mathrm{T}}\, Z^{-T}(j\omega)\Sigma^{\mathrm{T}} \tag{25}$$

where $Z(j\omega)$ is the matrix given by

$$Z(j\omega) = Ie^{j\omega\Delta t} - (I - KH)A \tag{26}$$

and I is the identity matrix. Equation (25) relates the power spectral densities of the components of the stress vector $\underline{\sigma}_k$ at various structural locations with the power spectral densities of the measured quantities involved in $\underline{y}_k$ available at the limited number of measured locations. This relation depends on the model (e.g. a finite element model) used to represent the behavior of the structure and the assumption that the excitation vector is broadband so that the excitations can be modeled by zero mean stationary white noise processes with spectral density described by $E[\underline{w}_k\underline{w}_l^{\mathrm{T}}] = Q\delta_{kl}$, where δ_{kl} is the Kronecker delta.

It should be noted that to apply (23), an estimate of the zero-lag covariance matrix R of the measurement noise and the zero-lag covariance matrix Q of the unknown input stochastic vector process has to be provided. The values of the covariance matrix R which have to be chosen, affects the estimates of the CPSD matrix $S_{\underline{\hat{\sigma}}}(\omega)$ in (25). However, an optimal estimate of the covariance matrix Q can be obtained using the strain measurements $\underline{y}(t)$ and the relation between the covariance matrix Q_{yy} of the measurement vector $\underline{y}(t)$ and the covariance matrix Q of the excitation process. Let $Q_{yy} \equiv Q_{yy}(Q)$ denote the relation between Q_{yy} and Q. Using (19) with $D = 0$ for strain measurements, this relation is given by

$$Q_{yy} = HQ_{xx}H^{\mathrm{T}} \tag{27}$$

where Q_{xx} is given by the discrete time Lyapunov equation for the system (18) in the form

$$AQ_{xx}A^{\mathrm{T}} - Q_{xx} + GQG^{\mathrm{T}} = 0 \tag{28}$$

The optimal values of the entries of the covariance matrix Q can be obtained by minimizing the difference between the covariance matrix $Q_{yy} \equiv Q_{yy}(Q)$ predicted by the linear model given Q and the covariance matrix $\hat{Q}_{yy} = (1/N_s)\sum_{k=1}^{N_s} \underline{y}_k\underline{y}_k^{\mathrm{T}}$ obtained from the measurements in $\underline{y}_k$, $k = 1, \cdots, N_s$. That is, the optimal value Q_{opt} is obtained by minimizing the objective function

$$J(Q) = tr\|Q_{yy}(Q) - \hat{Q}_{yy}\|^2 / tr\|\hat{Q}_{yy}\|^2 \tag{29}$$

with respect to the elements in Q. The optimal value Q_{opt} of Q is then substituted in (23) to completely define the Riccati equation (23). The solution P of the Riccati equation is substituted in (22) to find K, which is needed in (25). It should be noted that the optimal estimate of Q, as described above, assumes that the stochastic excitations in the vector process $\underline{w}_k$ are sufficiently broadband so that they can be adequately approximated by white noise processes. It should be noted that the size of the matrix Q increases as the number of excitation degree-of-freedom (DOF) increases. This increases the number of entries in Q to be estimated by minimizing equation (29) and may create identifiability problems. This problem can partly be alleviated by increasing the number of sensors placed in the structure.

3.3. Estimation of power spectral densities of stresses

The CPSD matrix $S_{\underline{y}}(\omega)$ of the sampled measurement vector $\underline{y}_k$, involved in (25), can be obtained using available signal processing techniques, such as the Welch technique [31,32]. Once $S_{\underline{y}}(\omega)$ has been estimated from the measurements, equation (25) can be used to estimate the CPSD $S_{\underline{\hat{\sigma}}}(\omega)$ of the stress response vector $\underline{\hat{\sigma}}_k$.

Alternatively, the PSD $S_{\underline{\hat{\sigma}}}(\omega)$ of the stress response vector $\underline{\hat{\sigma}}_k$ can be obtained by using equations (20) and (21) for the KF to provide estimates $\underline{\hat{x}}_k$ of the system state vector which are then used in equations (24) to estimate the stress vector $\underline{\hat{\sigma}}_k$. Finally, available signal processing techniques such as the Welch technique are used to compute the PSD $S_{\underline{\hat{\sigma}}}(\omega)$ from the sampled stress response vector $\underline{\hat{\sigma}}_k$.

The length of the sampled time history should be sufficiently large in order for the estimates to be accurate and also short enough to guarantee that the frequency content and the intensity

DOI: 10.1002/stc

of the response time histories do not change significantly with time. For very long ambient vibration time histories with time-varying frequency content and intensity, it might be necessary to apply the methodology over shorter time segments ensuring approximately the time invariance of the frequency content and intensity within each segment.

Once the CPSD matrix $S_{\underline{\hat{\sigma}}}(\omega)$ of the stress vector process $\underline{\hat{\sigma}}_k$ containing the stresses at all desirable structural locations is obtained, the diagonal elements diag$[S_{\underline{\hat{\sigma}}}(\omega)]$ of the matrix $S_{\underline{\hat{\sigma}}}(\omega)$ contain the PSD estimates required for fatigue predictions at these structural location using equations (2), (5) and (12).

4. APPLICATIONS

4.1. Spring-mass chain-like model

The applicability and effectiveness of the methodology is first illustrated using simulated 'measurements' from a simple class of N-DOF spring-mass chain-like model fixed at the two ends as shown in Figure 2. The model is used to represent a structure consisting of a series of bar and body elements as shown in Figure 3. The structure consists of N bodies with the ith body having mass m_i. The $i-1$ and the i bodies are connected by elastic bar elements which provide the stiffness to the system. The number of bar (or spring) elements of the chain model is $N+1$. The material of the bar elements is considered to be steel. For steel bar elements, the values of the fatigue constants in equation (4) are taken to be $c = 4.06 \times 10^{88}$ and $a = 9.82$. The ith bar element has length L_i, cross-sectional area A_i and modulus of elasticity E_i. For simplicity, each bar element is represented by a spring element with stiffness $k_i = E_i A_i / L_i$ as shown in Figure 2. In addition, the nodal mass m_i in Figure 2 includes the effect of the i body mass and the lumped mass arising from the bar elements connected to node i. The i component $q_i(t)$ of the vector $\underline{q}(t)$ corresponds to the displacement of the node i of the model. The system is subjected to an unmeasured excitation applied at node ρ. For the selected structure, the stress state at critical bar locations is uniaxial so that the fatigue prediction methodology can be directly applied.

Fatigue predictions from the KF methodology are based on a nominal model of the structure that corresponds to nominal stiffness values $k_i = k_{0,i}$. The measurements that are collected from the actual structure are generated from a reference model introduced to simulate the actual behavior of the structure. To study the effects of the model error on the accuracy of the KF method for fatigue predictions, the reference model is selected to be different from the nominal model. Specifically, the reference model corresponds to the model shown in Figure 2 with stiffness values perturbed from the nominal stiffness values according to the expression $k_i = k_{0,i}(1+n_i)$, where $k_{0,i}$ are the nominal values used in KF-based fatigue predictions and $n_i \sim N(0, s_i^2)$ are samples from a zero mean normal distribution with variance s_i^2. The standard deviation s_i of the perturbed terms controls the size of the model error and reflects the

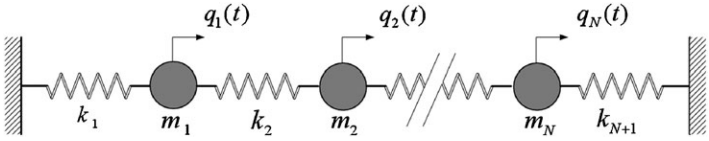

Figure 2. N-DOF spring-mass chain-like model.

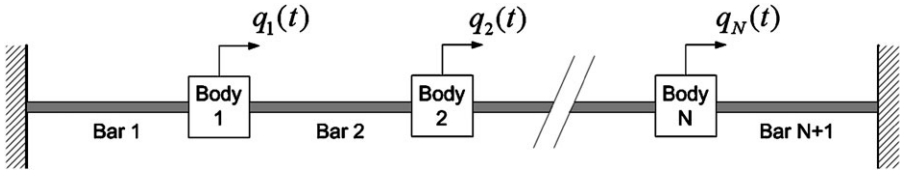

Figure 3. Structure consisting of a series of N masses and $N+1$ bar elements.

DOI: 10.1002/stc

differences observed in real applications between the predictions from a model of a structure and the actual behavior of the structure.

The measurements are assumed to be strain measurements. These measurements are simulated from the reference model of the structure using two types of excitations, referred to as Type I and Type II excitations. Type I excitations are assumed to be samples of a Gaussian white noise process, thus providing good approximation to an excitation whenever its correlation time is sufficiently small compared with the system time constants. In this case, the excitation vector $\underline{u}(t)$ is modeled by samples generated by a Gaussian stationary white noise vector process $\underline{n}(t)$ with constant spectral density matrix $S_{\underline{u}} = S_0$. Type II excitations are assumed to be samples of a unimodal filtered white noise excitation with characteristics given by the second-order filter equation

$$\ddot{q}_f(t)+2\zeta_f\omega_f\dot{q}_f(t)+\omega_f^2 q_f(t) = n(t) \tag{30}$$

$$u(t) = \ddot{q}_f(t) = -2\zeta_f\omega_f\dot{q}_f(t) - \omega_f^2 q_f(t)+n(t) \tag{31}$$

The characteristics of the excitation depend on the values of the filter parameters: the dominant frequency ω_f and the damping ratio ζ_f. The value of the PSD S_0 of the Gaussian stationary white noise process $n(t)$ controls the intensity of the excitation samples $u(t)$ generated by the second-order filter.

For type I excitation, the discrete state space formulation of the equations of motion for the reference model is used to simulate response time history data as well as compute estimates of the covariance responses and the PSD of the responses using the white noise excitation $n(t)$ applied at node ρ. For type II excitation, the responses from the reference model can readily be obtained by a discrete state space formulation of an augmented system which consists of the equations of motion (13) and the filter equations (30)–(31) excited by the white noise process $n(t)$. In this augmented system, the system states include the states of the original system in (14) and the filter states arising from (30). For both excitation types, the strain and stress response time histories $\underline{\varepsilon}_k$ and $\underline{\sigma}_k$, respectively, are simulated at all bar elements using the discrete state space formulation. The time discretization step used in simulating the sampled data is $\Delta t = 0.5 \times 10^{-3}$. The simulated strain and stress response time histories are the reference stress response time histories that are considered to be the exact stress response time histories for the excitations used. These response time histories and the corresponding power spectral densities are also used with the fatigue methodology in Section 2 to compute the damage accumulation and lifetime of the entire body of the structure due to fatigue. Such predictions constitute the reference (exact) predictions against which the predictions from the proposed KF approach should be compared with for assessing the accuracy of the proposed methodology.

For convenience, the set o is introduced that contains the bar element numbers where the strains are measured. The measured strain response time histories $\underline{y}_k = \underline{\varepsilon}_k^{(o)}$ are the components of the reference response time history vector $\underline{\varepsilon}_k$ associated with the bar element numbers identified in the set o. In practice, these measurements are collected using appropriate sensors, such as strain gauges. Let p be the set that contains the bar element numbers where the stresses will be predicted. In this study, the set p is selected to be $p = \{1,\ldots,N+1\}$, i.e. it is assumed that stresses are predicted at all bar elements.

4.1.1. Five DOF model. Results demonstrating the effectiveness of the proposed methodology are first presented for a five-DOF system ($N = 5$), as shown in Figure 2. The nominal values of the nodal masses are $m_1 = m_5 = 21\,\text{kg}$, $m_2 = m_4 = 15\,\text{kg}$ and $m_3 = 12\,\text{kg}$. A uniform distribution of the properties of the bar elements is assumed resulting in uniform stiffness $k_i = k_0$, $i = 1,\ldots,N$. The nominal values of the stiffness properties are chosen so that $k_0 = E_0A_0/L_0$, where $E_0 = 2.1 \times 10^{11} N/m^2$, $A_0 = \pi(0.0035)^2 m^2$ and $L_0 = 0.3\,m$ are same for all bar elements. For the mass and bar properties selected, the nominal values of the natural frequencies of the five-DOF system are 110.0, 193.4, 277.0, 344.3 and 425.3 Hz. The damping matrix C in the equations of motion (13) is chosen assuming that the system is classically damped. Specifically, the damping matrix C is selected so that the values of the modal damping ratios are 1% for all

DOI: 10.1002/stc

contributing modes. A single excitation is considered which is applied at node $\rho = 5$. The measured strain response time histories $\underline{y}_k = \underline{\varepsilon}_k^{(o)}$ at the bar elements identified by the set o are used to predict the stress response time histories at all bar elements identified in the set p using the proposed KF approach. These predictions depend on the values of the measurement noise covariance R in the KF formulation. In this study, the noise covariance matrix R is selected to be a diagonal matrix of the form $R = \eta^2 \text{diag}(\hat{Q}_{yy})$, where ε gives the level of the observation error and $\text{diag}(\hat{Q}_{yy})$ denotes the diagonal matrix formed from $\hat{Q}_{yy}$ after setting the non-diagonal terms to zero. In the numerical results that follow, the values of $\eta = 0.1\%$ and $\eta = 10\%$ are used which corresponds to very small and relatively large observation errors, respectively.

The simulated measurements and the reference fatigue predictions are first obtained for the Type I white noise excitation. For demonstration purposes, comparison between the reference (exact) stress PSD simulated by the model and the estimated PSD from the KF are given in Figure 4 for the bar elements $p = \{2, 4, 6\}$, assuming that the measured strains are at bar elements $o = \{1, 2\}$. Results are presented for the case of relatively large model error ($s_i = 5\%$) in Figure 4(a, b) at bar elements 2 and 4 and for the case of zero model error ($s_i = 0$) in Figure 4(c, d) at bar elements 4 and 6. It can be seen in Figure 4(a) for the case of relatively large model error that the estimated PSDs of the stress at the bar element 2, where measurements are available, almost coincides with the corresponding reference stress PSDs simulated by the model. At the bar element 4, where measurements are not available, there is a discrepancy between the estimated and reference (exact) stress PSDs, as shown in Figure 4(b). For the case of relatively large model error, the discrepancies observed in Figure 4(b) are mainly due to the fact that the nominal model used for PSDs predictions from the KF approach differs from the reference model used to simulate the reference PSDs. The size of the discrepancies depends on the size of the model error. Specifically, these discrepancies, shown in Figure 4(b) for relatively

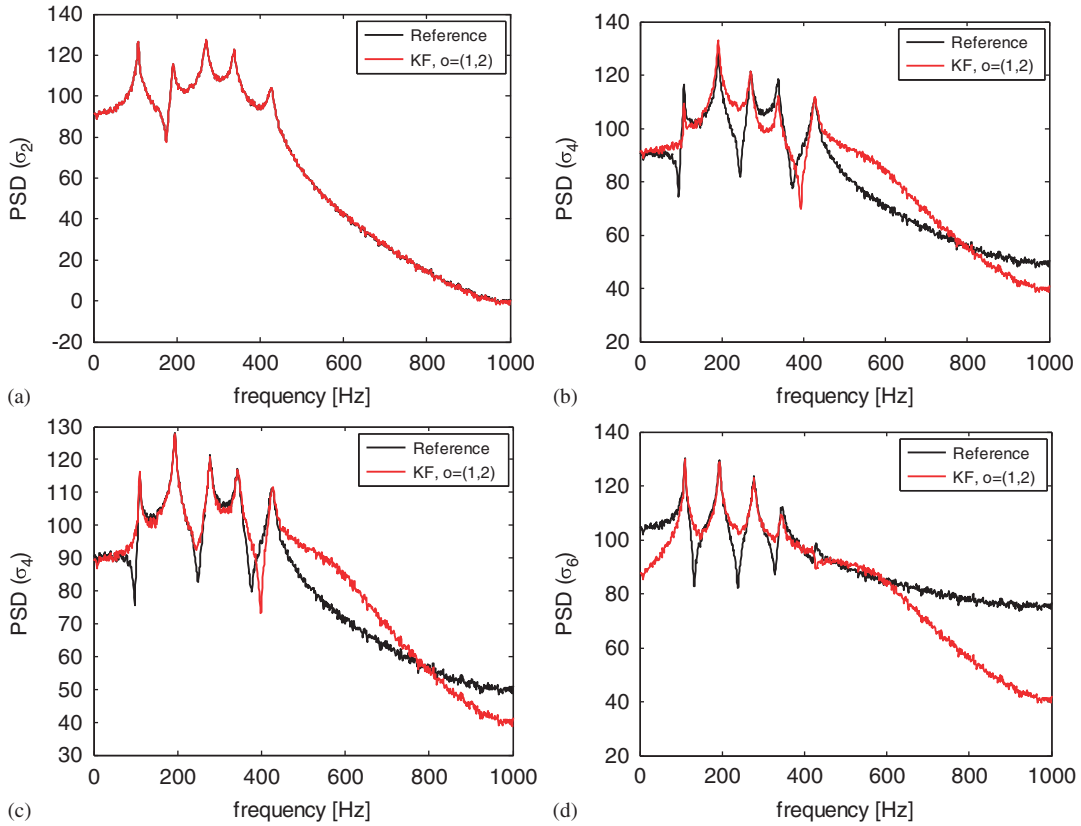

Figure 4. Comparison between reference and estimated from KF PSD of the stress response at bar elements 2, 4 and 6; (a,b) relatively large model error $s = 5\%$, (c,d) zero model error $s = 0\%$.

DOI: 10.1002/stc

large model error ($s_i = 5\%$), are found to be significantly higher than the discrepancies observed in Figure 4(c) for zero model error ($s_i = 0$). For zero model error, the discrepancies shown in Figure 4(c, d) for bar elements 4 and 6, respectively, are due to the estimation error associated with the KF. However, it should be noted that the predictions of the PSD from the KF approach are quite good, especially for the high amplitudes around the resonance peaks, which mainly contribute to the fatigue process.

Lifetime predictions due to fatigue are next compared in Figure 5(a–d) for all six bar (spring) elements of the structure. The lifetime values in these figures are obtained using the fatigue prediction formula (5). For each bar element, there are six lifetime fatigue predictions. The first prediction is based on the reference time histories simulated by the reference model and it is used as the exact value against which to study the accuracy of the predictions from the proposed KF methodology. The other five fatigue-based lifetime estimates are the ones predicted by the methodologies based on the use of KF method and the nominal model to estimate the stress response time histories at all bar elements. To study the effect of the number and location of sensors on the accuracy of the predictions, the five fatigue lifetime estimates shown in Figure 5(a–d) correspond to the following five sensor configurations that differ from the number and location of sensors used: one sensor configuration $o = \{6\}$ involving one sensor placed at location or bar element 6, two sensor configurations $o = \{1, 2\}$ and $o = \{3, 4\}$ each one involving two sensors placed at locations denoted in the set o, and two sensor configurations $o = \{1, 2, 3\}$ and $o = \{2, 3, 4\}$ each one involving three sensors. To study the effect of model error on the accuracy of the KF methodology, the results in Figure 5(a–c) are based on simulated measurements from the reference model chosen to involve zero ($s_i = 0$), moderate

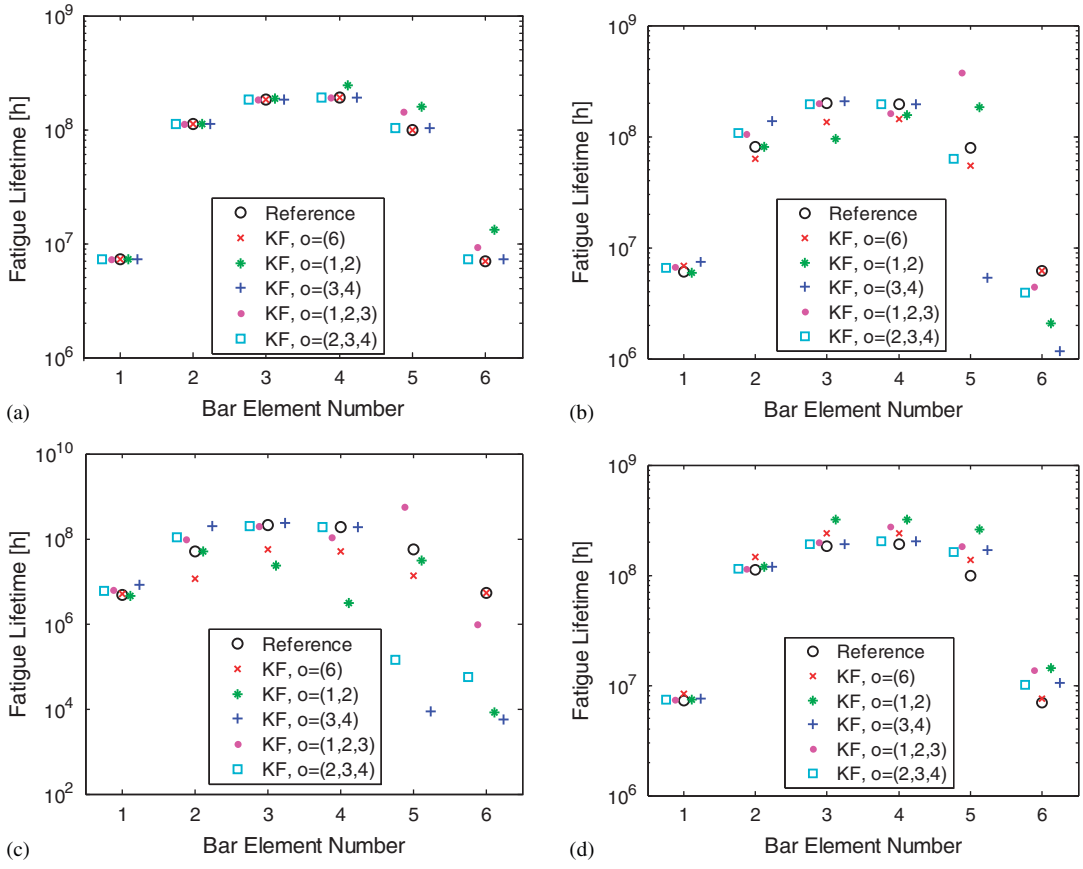

Figure 5. Comparison of reference fatigue-based lifetime estimates and the estimates predicted by the KF for the $N = 5$ DOF model as a function of the number and location of sensors: (a) $s_i = 0$, $\eta = 0$; (b) $s_i = 2\%$, $\eta = 0$; (c) $s_i = 5\%$, $\eta = 0$; and (d) $s_i = 0$, $\eta = 10\%$.

DOI: 10.1002/stc

($s_i = 2\%$) and relatively large ($s_i = 5\%$) model error, while the observation error used for KF-based fatigue predictions is negligible ($\eta = 0.1\%$). To study the effect of observation error in the accuracy of the KF methodology, the results in Figure 5(d) are based on simulated measurements from the reference model chosen to involve zero model error ($s_i = 0$) and relatively large observation error ($\eta = 10\%$) used for KF-based fatigue predictions.

It can be seen from the results for the fatigue predictions involving zero model error ($s_i = 0$) shown in Figure 5(a) that the estimates based on the KF predictions are quite close to the reference fatigue values obtained from the actual (reference) response time histories. It also becomes clear that the accuracy of the KF predictions depend on the number and location of sensors in the structure. Specifically, the best predictions are obtained from one sensor placed at bar element 6. Similar accuracy in the predictions are obtained from the sensor configurations $o = \{3, 4\}$ and $o = \{2, 3, 4\}$ involving two and three sensors. However, the sensor configurations $o = \{1, 2\}$ and $o = \{1, 2, 3\}$ provide significantly less accurate predictions in the entire structure (all six bar elements) than the predictions provided by one sensor placed at location 6. Specifically, significant discrepancies between the reference and KF fatigue predictions from the sensor configurations $o = \{1, 2\}$ and $o = \{1, 2, 3\}$ are observed in bar element 5 and 6. It becomes evident from the results in Figure 5(a) that the locations and number of sensors affect the accuracy of the fatigue lifetime predictions from the proposed KF approach. Optimal sensor location methodologies [33] may be advantageously used to obtain the most informative locations that give the best accuracy in the fatigue lifetime predictions with the least number of sensors.

Comparing the results in Figure 5(a–c) corresponding to zero ($s_i = 0$), moderate ($s_i = 2\%$) and larger ($s_i = 4\%$) model errors, it is evident that the size of model error affects the accuracy of the fatigue prediction provided by the proposed KF methodology. For a fixed sensor configuration, the accuracy of the fatigue predictions obtained from the KF methodology deteriorates as the size of the model error increases. Moreover, the accuracy of the predictions depends highly on the number and location of sensors. There are optimal sensor locations, which give the most accurate fatigue predictions. Specifically, the most accurate predictions in the entire structure for the case of moderate model error ($s_i = 2\%$) are obtained from sensor configurations $o = \{6\}$ and $o = \{2, 3, 4\}$ involving one and three sensors, respectively. For the case of larger model error ($s_i = 5\%$), the most accurate predictions in the entire structure (all bar elements) are obtained from sensor configurations $o = \{6\}$ involving one sensor, followed by the predictions provided by the sensor configuration $o = \{1, 2, 3\}$ involving three sensors.

The effect of measurement error on the fatigue predictions provided by the KF approach is next considered by comparing the results in Figure 5(d) obtained for relatively large observation error of the order of $\eta = 10\%$ with the results in Figure 5(a–c) obtained for very small ($\eta = 0.1\%$) observation error. It can be seen that the accuracy of the fatigue predictions is less sensitive to the magnitude of the observation error than it is to the magnitude of the model error. In addition, the accuracy of the fatigue lifetime predictions provided by the KF for the different sensor configurations observed in Figure 5(d) for zero model error and significant observation error ($\eta = 10\%$) does not significantly deteriorate when compared with the accuracy of the predictions observed in Figure 5(a) provided by the methodology for zero model error and very small ($\eta = 0.1\%$) observation error.

Next, results are also presented for simulated measurements generated from the Type II filtered white noise excitation. In this case, one examines the effect of the characteristics of the excitation on the accuracy of the proposed methodology. As before, the excitations is applied at node $\rho = 5$. Figure 6 compares the reference fatigue estimates and the fatigue predictions provided by the KF methodology for three different excitation characteristics: broadband excitation corresponding to values $\omega_f = 200\,\text{Hz}$ and $\zeta_f = 0.4$ (Figure 6(a)), and two lightly damped excitations ($\zeta_f = 0.02$) with resonant frequencies close to the first, $\omega_f = \omega_1 \approx 110\,\text{Hz}$ (Figure 6(b)), and third $\omega_f = \omega_3 \approx 277\,\text{Hz}$ (Figure 6(c)), natural frequency of the structure. All results shown in Figure 6(a–c) are based on simulated measurements that involve zero model error ($s_i = 0$) and negligible measurement error $\eta = 0.1\%$. The results in Figure 6(d) are based on large model error ($s_i = 5\%$) and for the lightly damped excitation ($\zeta_f = 0.02$) with

DOI: 10.1002/stc

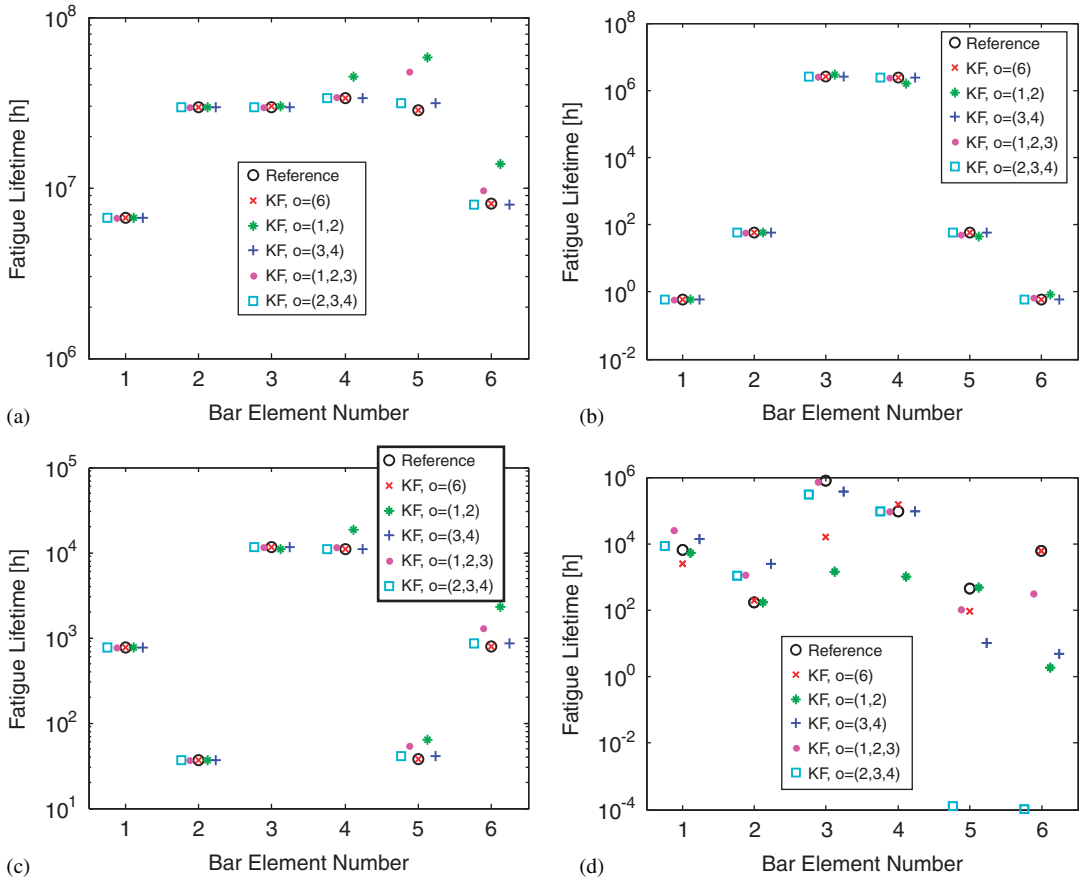

Figure 6. Comparison of reference fatigue-based lifetime estimates and the estimates predicted by the KF for the $N = 5$ DOF model as a function of the number and location of sensors: (a) $\omega_f = 200\,\text{Hz}$, $\zeta_f = 0.4$, $s_i = 0$; (b) $\omega_f = \omega_1 \approx 110\,\text{Hz}$, $\zeta_f = 0.02$, $s_i = 0$; (c) $\omega_f = \omega_3 \approx 277\,\text{Hz}$, $\zeta_f = 0.02$, $s_i = 0$; and (d) $\omega_f = \omega_3 \approx 277\,\text{Hz}$ and $\zeta_f = 0.02$, $s_i = 5\%$.

resonant frequency close to the third $\omega_f = \omega_3 \approx 277\,\text{Hz}$ natural frequency of the structure. All filtered white noise excitations correspond to the same variance. Given the values of ω_f and ζ_f, this is achieved by selecting appropriately the intensity of the white noise $n(t)$ so that the output $u(t)$ in (31) has the desired value of variance.

It is clear in Figure 6(a–c) that for the case of zero model error, the KF methodology gives very good predictions for a variety of excitation characteristics, including broadband and lightly damped excitations. As before, the accuracy of the predictions depends on the number and location of sensors. The most accurate predictions are obtained from the sensor configuration $o = \{6\}$ involving one sensor placed at location (bar element) 6, followed by the sensor configurations $o = \{3,4\}$ and $o = \{2,3,4\}$ involving two and three sensors. Less accurate predictions are obtained from the sensor configurations $o = \{1,2\}$ and $o = \{1,2,3\}$ involving two and three sensors, respectively. Obviously, optimizing the sensor placement in the structure can significantly improve the accuracy of the fatigue lifetime predictions provided by the KF methodology. Comparing the fatigue prediction results given in Figure 6(d) for large model error $s_i = 5\%$ to the fatigue prediction results in Figure 6(c) for zero model error, it is clear that the accuracy of the predictions from the KF methodology deteriorates as the model error increases. Sensor configuration $o = \{6\}$ involving one sensor provides predictions with the best accuracy compared with the predictions provided by all other sensor configurations used in Figure 6.

For the two lightly damped excitations shown in Figure 6(b, c), it is observed that the fatigue at each bar element depends on the mode excited. For the excitation with dominant frequency close to the first natural frequency (Figure 6(b)), the structure responds mainly to its first mode

DOI: 10.1002/stc

and the strains levels due to vibration, depending on the derivatives of the modeshape, are higher at bar elements 1 and 6, while due to symmetry they are lower at the middle bar elements 3 and 4. Consequently, the bar elements 1 and 6 are expected to have significantly less fatigue lifetime, whereas the middle bar elements 3 and 4 are expected to have high fatigue lifetime, which is consistent with the results observed in Figure 6(b). For the excitation with dominant frequency close to the third natural frequency, the structure respond mainly with its third mode and therefore high strain values are expected also to occur at internal bar elements 2 and 5, while due to symmetry the strains at the middle elements 3 and 4 are expected to be small. This is consistent with the small fatigue lifetime values predicted for the bar elements 2 and 5 and the high fatigue lifetime values predicted for the middle bar elements 3 and 4, as shown in Figure 6(c).

4.1.2. Twenty DOF model. Finally, results demonstrating the effectiveness of the proposed methodology are presented for a 20-DOF system ($N = 20$), as shown in Figure 2. The nodal masses are assumed to be the same, i.e. $m_i = m_0$, $i = 1, \ldots, N$. A uniform distribution of the properties of the bar elements is also assumed resulting in uniform stiffness $k_i = k_0$, $i = 1, \ldots, N$. The nominal values of the mass and stiffness properties are chosen so that $m_0 = 30\,\text{kg}$ and $k_0 = E_0 A_0 / L_0$, where $E_0 = 2.1 \times 10^{11}\text{N/m}^2$, $A_0 = \pi(0.0035)^2 m^2$ and $L_0 = 0.3\,\text{m}$ are same for all bar elements. For the mass and bar properties selected, the nominal values of the natural frequencies of the 20-DOF system range from 22.5 (minimum) to 300.8 Hz (maximum). The structure is subjected to either Type I stationary white noise excitation or Type II non-white excitation applied at node $\rho = 10$, with constant spectral density matrix equal to $S_{\underline{u}} = S_0 = 10$. The strain response time histories $\underline{y}_k = \underline{\varepsilon}_k^{(o)}$ at the measured DOFs are used to predict the stress response time histories at all bar elements identified in the set $p = \{1, \ldots, 21\}$ using the KF approach.

Lifetime predictions due to fatigue are shown in Figure 7 for all 21 bar (spring) elements of the structure. For each bar element, there are six lifetime fatigue predictions. The first prediction is based on the reference time histories simulated by the reference model and it is used as the exact value against which to study the accuracy of the predictions from the proposed KF methodology. The second fatigue lifetime prediction is based on the use of KF method and the nominal model using sensors at all 21 bar elements. This second prediction uses measurements from all 21 bar elements and thus represents the most accurate results that can be obtained from the KF methodology. The other four fatigue-based lifetime estimates are the ones predicted by the methodologies based on the use of KF method and the nominal model to estimate the stress response time histories at all bar elements using a limited number of sensors. To study the effect of the number and location of sensors on the accuracy of the predictions, the four fatigue lifetime estimates shown in Figure 7(a–d) in the entire structure (all 21 bar elements) correspond to the following four sensor configurations that differ from the number and location of sensors used: one sensor configuration $o = \{10\}$ involving one sensor placed at location or bar element 10, one sensor configuration $o = \{5, 21\}$ involving two sensors placed at locations 5 and 21, one sensor configuration $o = \{5, 10, 21\}$ involving three sensors, and one sensor configuration $o = \{1, 5, 16, 21\}$ involving four sensors. Figure 7(a) compares results for white noise excitation, Figure 7(b) compares results for broadband-filtered white noise excitation ($\omega_f = 110\,\text{Hz}$, $\zeta_f = 0.6$), while Figure 7(c, d) compares results for lightly damped filtered white noise excitations ($\zeta_f = 0.02$) with dominant frequency close to the second natural frequency of the structure ($\omega_f = \omega_2 \approx 44\,\text{Hz}$). Predictions in Figure 7(a–c) correspond to moderate model error ($s_i = 2\%$) and very small observation error ($\eta = 0.1\%$). To study the effect of observation error in the accuracy of the KF methodology, predictions in Figure 7(d) correspond to zero model error ($s_i = 0\%$) and large observation error ($\eta = 10\%$).

It can be seen that despite the moderate model error considered in Figure 7(a–c) and the large measurement error considered in Figure 7(d), the fatigue lifetime prediction values provided by the KF approach for a full sensor configuration involving 21 sensors installed in all 21 bar elements are quite close to the reference fatigue lifetime values. For given excitation case, it becomes clear that the accuracy of the fatigue lifetime predictions based on the KF approach using fewer than 21 sensors depend on the number and location of sensors in the structure. Specifically, the best predictions are obtained from the sensor configuration $o = \{10\}$ involving one sensor located at element 10 and the sensor configuration $o = \{5, 10, 21\}$ involving three

DOI: 10.1002/stc

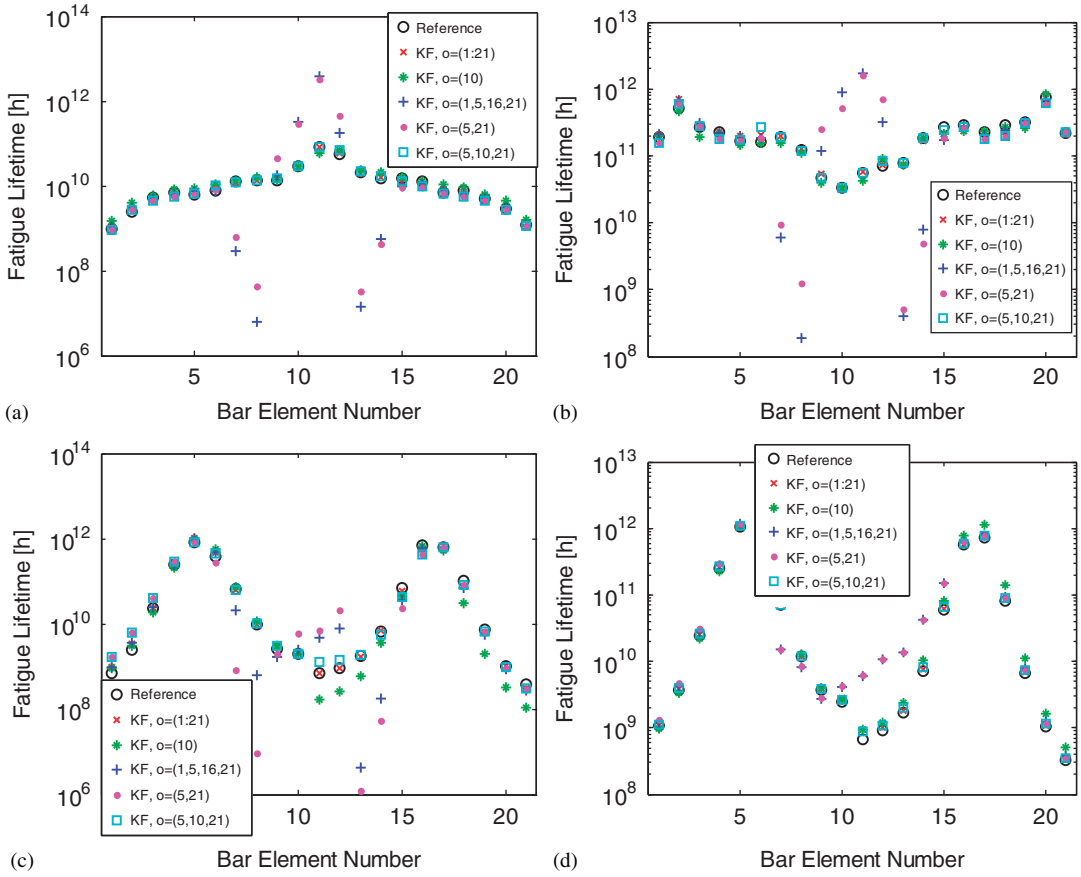

Figure 7. Comparison of reference fatigue-based lifetime estimates and the estimates predicted by the KF for the $N = 20$ DOF model as a function of the number and location of sensors: (a) white noise, $s_i = 2\%$, $\eta = 0.1\%$; (b) $\omega_f = 110\,\text{Hz}$, $\zeta_f = 0.6$, $s_i = 2\%$, $\eta = 0.1\%$; (c) $\omega_f = \omega_2 \approx 44\,\text{Hz}$, $\zeta_f = 0.02$, $s_i = 2\%$, $\eta = 0.1\%$; and (d) $\omega_f = \omega_2 \approx 44\,\text{Hz}$, $\zeta_f = 0.02$, $s_i = 0\%$, $\eta = 10\%$.

sensors located at elements 5, 10 and 21. Such predictions are quite close to the reference fatigue values obtained from the actual (reference) response time histories and to the KF prediction provided by a full sensor configuration involving 21 sensors. It should be noted that the sensor configuration $o = \{5, 10, 21\}$ gives slightly better fatigue lifetime prediction accuracy at all 21 bar elements than the sensor configuration $o = \{10\}$. This is due to the fact that the sensor configuration $o = \{5, 10, 21\}$ contains the sensor configuration $o = \{10\}$ and in addition it involves two extra sensors that provide additional information for reconstructing more accurately the response at unmeasured locations. However, the sensor configurations $o = \{5, 21\}$ and $o = \{1, 5, 16, 21\}$ involving two and four sensors, respectively, provide significantly less accurate predictions, especially at the bar elements 7 to 14, than the predictions provided by the sensor configurations $o = \{10\}$ and $o = \{5, 10, 21\}$ involving one and three sensors, respectively. It thus becomes evident from the results in Figure 7 that the location and number of sensors affect the accuracy of the fatigue lifetime predictions. Optimal sensor location strategies [33] may be advantageously used to obtain the most informative locations that give the best accuracy in the fatigue lifetime predictions with the least number of sensors.

The relative importance of the model and measurement error on the accuracy of the fatigue predictions provided by the KF is investigated by comparing the results in Figure 7(d) obtained for relatively large observation error of the order of $\eta = 10\%$ and zero model error with the results in Figure 7(c) obtained for very small ($\eta = 0.1\%$) observation error and moderate model error ($s_i = 2\%$). It can be seen from these figures that the accuracy of the fatigue predictions are less sensitive to the size of the observation error. Specifically, the accuracy of the fatigue lifetime

DOI: 10.1002/stc

predictions provided by the KF for the different sensor configurations observed in Figure 7(d) for zero model error and significant observation error ($\eta = 10\%$) does not significantly deteriorate when compared with the accuracy of the predictions observed in Figure 7(c) provided by the methodology for moderate model error ($s_i = 2\%$) and very small observation error ($\eta = 0.1\%$).

4.2. Truss model

Next, the effectiveness of the methodology is illustrated using simulated 'measurements' from a two-dimensional truss structure shown in Figure 8. The dimensions of the truss are $L = h = 1.0\,\text{m}$. The truss consists of $N = 35$ elastic steel truss elements and 14 DOFs. All truss element have cross-sectional areas $A_i = A_0$ and modulus of elasticity $E_i = E_0 = 2.1 \times 10^{11}\,\text{N/m}^2$, $i = 1, \ldots, N$. A nodal mass m_i is added at all truss nodes and the nominal values of the nodal masses are selected to be $m_0 = 200\rho A_0 L$, where $\rho = 7850\,\text{kg/m}^3$ is the steel density. The nominal stiffness of each truss element is obtained from $k_i = E_0 A_0 / L_i$, $i = 1, \ldots, N$, where L_i is the length of the ith element. For the mass and stiffness properties selected, the nominal values of the natural frequencies of the truss range from 1.72 (minimum) to 129.6 Hz (maximum). The structure is assumed to be classically damped with the damping matrix C selected so that the values of the modal damping ratios are 5% for all contributing modes.

Fatigue predictions from the KF methodology are based on the nominal model of the structure that corresponds to nominal nodal mass values $m_i = m_0$. To study the effects of the model error on the accuracy of the KF method for fatigue predictions, the measurements are generated from the reference model obtained by perturbing the nodal mass values from the nominal modal mass values according to the expression $m_i = m_0(1+n_i)$, where m_0 are the nominal values used in KF-based fatigue predictions and $n_i \sim N(0, s_i^2)$ are samples from a zero mean normal distribution with variance s_i^2.

The structure is subjected to either Type I stationary white noise excitation or Type II non-white excitation applied at the right end as shown in Figure 8. The constant spectral density of the white noise is selected to be $S_{\underline{u}} = S_0 = 2(\rho A_0 L g)^2$, where g is the acceleration of gravity. The measurements are assumed to be strain measurements at the truss elements.

Lifetime predictions due to fatigue are shown in Figure 9 for all 35 truss elements of the structure. For each truss element, there are six lifetime fatigue predictions. The first prediction is based on the reference time histories simulated by the reference model and it is used as the exact value against which to study the accuracy of the predictions from the proposed KF methodology. The second fatigue lifetime prediction represents the most accurate prediction that can be obtained from the KF methodology using sensors at all 35 truss elements. To study the effect of the number and location of sensors on the accuracy of the predictions, the other four fatigue-based lifetime estimates are the ones predicted by the KF method based on the nominal model to estimate the stress response time histories at all bar elements using the sensor configurations SC-1, SC-2, SC-3 and SC-4, as shown in Figure 10. These sensor configurations involve a limited number of three (SC-1 and SC-2) and six (SC-3 and SC-4) sensors placed at various locations. Figure 9(a, b) compares results for white noise excitation and for moderate ($s_i = 2\%$) and relatively large ($s_i = 5\%$) model error, respectively. Figure 9(c, d) compares results for lightly damped filtered white noise excitations ($\zeta_f = 0.05$) with dominant frequency close to the first

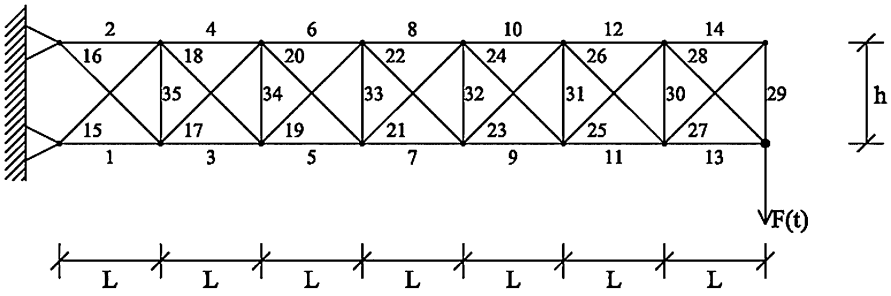

Figure 8. Two-dimensional truss model consisting of 35 truss elements.

DOI: 10.1002/stc

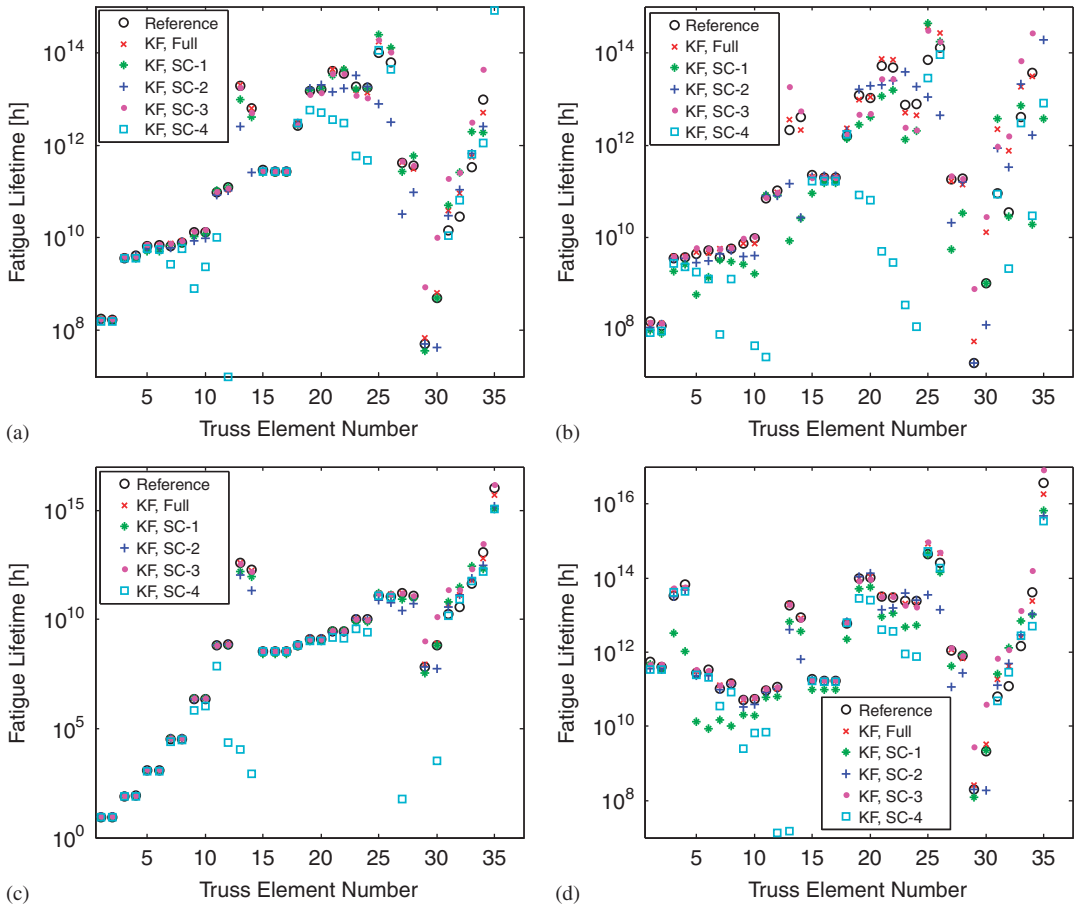

Figure 9. Comparison of reference fatigue-based lifetime estimates and the estimates predicted by the KF for the truss model as a function of the number and location of sensors: (a) white noise, $s_i = 2\%$; (b) white noise, $s_i = 5\%$; (c) $\omega_f = \omega_1 \approx 1.92\,\text{Hz}$, $\zeta_f = 0.05$, $s_i = 2\%$; and (d) $\omega_f = \omega_3 \approx 13.1\,\text{Hz}$, $\zeta_f = 0.05$, $s_i = 2\%$.

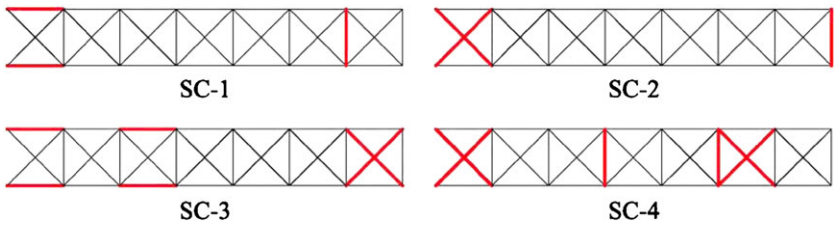

Figure 10. Sensor configurations SC-1, SC-2, SC-3 and SC-4 involving three and six sensors (thick line elements denote the truss elements monitored with strain sensors).

($\omega_f = \omega_1 \approx 1.72\,\text{Hz}$) and third ($\omega_f = \omega_3 \approx 13.1\,\text{Hz}$) natural frequency of the structure, respectively. Predictions in Figure 9(c, d) correspond to moderate model error ($s_i = 2\%$). All predictions in Figure 9(a–d) correspond to very small observation error ($\eta = 0.1\%$).

It can be seen that despite the moderate model error ($s_i = 2\%$) considered in Figure 9(a, c and d), the fatigue lifetime prediction values provided by the KF approach for a full sensor configuration installed at all 35 truss elements are quite close to the reference fatigue lifetime values. The larger differences that are observed for the vertical members 29 to 35 of the truss are due to the size of model error ($s_i = 2\%$) considered. For relatively large model error ($s_i = 5\%$), the accuracy of the predictions from the KF approach for a full sensor configuration, shown in Figure 9(b), tend to overall deteriorate, especially for the vertical members 29 to 35.

DOI: 10.1002/stc

It becomes clear that the accuracy of the fatigue lifetime predictions based on the KF approach using fewer than 35 sensors depend on the number and location of sensors in the structure. Specifically, the best predictions in Figure 9(a, c and d) corresponding to moderate model error ($s_i = 2\%$) are obtained from the sensor configurations SC2 and SC3, involving three and six sensors, respectively. SC-3 provides more accurate KF-based fatigue predictions for the horizontal (1 to 14) and the diagonal (15 to 28) elements than the fatigue predictions estimated by SC-2. The SC-3 predictions are relatively close to the reference fatigue values obtained from the actual (reference) response time histories and to the KF prediction provided by a full sensor configuration involving 35 sensors. SC-2 provides more accurate fatigue predictions than SC-3 for the horizontal members 29 to 35. The sensor configuration SC-1 involving three sensors gives less accurate predictions than the sensor configurations SC-2 and SC-3. Finally, the sensor configuration SC-4 involving six sensors, provide overall significantly less accurate predictions at several truss elements than the predictions provided by the sensor configuration SC-2 involving three sensors. It thus becomes evident from the results in Figure 9 that the location and number of sensors affect the accuracy of the fatigue lifetime predictions.

Comparing the results for moderate and large model error in Figure 9(a, b), respectively, the accuracy of the predictions from the sensor configurations involving three and six sensors deteriorate, as the model error increases from $s_i = 2\%$ to $s_i = 5\%$. However, for the horizontal members and a number of the diagonal members, the accuracy of the fatigue lifetime predictions remains within acceptable levels. It should be noted that for zero model error the predictions for all sensor configurations are extremely good at all truss elements. Such predictions are not shown in Figure 9 because they coincide with the reference fatigue values.

5. CONCLUSIONS

A methodology for estimating damage due to fatigue on the entire body of a structure, using spectral methods and output-only vibration measurements at a limited number of locations, was presented. The fatigue predictions presented in this study were illustrated for structural members subjected to a uniaxial stress state. These predictions can be extended using available methods [19,20] to structural members subjected to multiaxial stress state. Using the available response time history measurements and a model of the structure, a KF approach was used for predicting the power spectral densities of the stresses in the entire body of the structure needed in the spectral-based fatigue prediction methodology. These PSD predictions were used to construct fatigue accumulation and lifetime prediction maps consistent with measurements provided by a monitoring system. Simulated measurements from a spring-mass chain-like structure and a truss structure suggest that the proposed methodology for lifetime fatigue prediction provide sufficiently accurate estimates even for the cases where the broadband assumptions of the stochastic excitation processes are violated. In particular, systematic numerical studies have demonstrated that the accuracy of the proposed methodology depends on the size of the model and observation errors, as well as the number and location of sensors.

The proposed method can also be seen as a tool for a lifetime prognosis within structural health monitoring concepts. Specifically, the proposed method can be used to estimate the accumulation of damage due to fatigue during operation in the entire body of a structure taking into account the actual conditions collected from a sensor network placed at limited number of locations. The fatigue accumulation and lifetime predictions provided by the proposed methodology are useful for designing optimal maintenance strategies for most critical components of metallic structures using information collected from a sensor network.

ACKNOWLEDGEMENTS

This research was funded by the Greek National Scholarship Foundation (IKY) within the IKYDA program framework and by the Deutscher Akademischer Austausch Dienst (DAAD, German Academic Exchange Service) within the PPP program. This research is also part of the 03-ED-524 project,

DOI: 10.1002/stc

implemented within the framework of the 'Reinforcement Programme of Human Research Manpower' (PENED) and co-financed 25% from the Greek Ministry of Development (General Secretariat of Research and Technology) and 75% from E.U. (European Social Fund).

REFERENCES

1. Palmgren A. Die Lebensdauer von Kugallagern. *VDI-Zeitschrift* 1924; **68**(14):339–341.
2. Miner MA. Cumulative damage in fatigue. *Applied Mechanics Transactions* (*ASME*) *1945; **12**(3):A159–A164*.
3. Lutes LD, Sarkani S. *Random Vibrations*: *Analysis of Structural and Mechanical Systems*. Elsevier Butterworth-Heinemann: Oxford, 2004.
4. Wirsching PH, Light MC. Fatigue under wide band random stress. *Journal of Structural Engineering* (*ASCE*) 1980; **106**(7):1593–1607.
5. Lutes LD, Corazao M, Hu S-LJ, Zimmerman J. Stochastic fatigue damage accumulation. *Journal of Structural Engineering* (*ASCE*) 1984; **110**(11):2585–2601.
6. Lutes LD, Larsen CE. Improved spectral method for variable amplitude fatigue prediction. *Journal of Structural Engineering* (*ASCE*) 1990; **116**(4):1149–1164.
7. Rychlik I. On the 'narrow-band' approximation for expected fatigue damage. *Probabilistic Engineering Mechanics* 1993; **8**:1–4.
8. Dirlik T. Applications of computers to fatigue analysis. *Ph.D. Thesis*, Warwick Univ., 1985.
9. Benasciutti D, Tovo R. Comparison of spectral methods for fatigue analysis of broad-band Gaussian random processes. *Probabilistic Engineering Mechanics* 2006; **21**:287–299.
10. Chaudhury GK, Dover WD. Fatigue analysis of offshore platforms subject to sea wave loading. *International Journal of Fatigue* 1985; **7**(1):13–19.
11. Chow CL, Li DL. An analytical solution for fast fatigue assessment under wide band random loading. *International Journal of Fatigue* 1991; **13**:395–404.
12. Larsen CE, Lutes LD. Predicting the fatigue life of offshore structures by the single-moment spectral method. *Probabilistic Engineering Mechanics* 1991; **6**(2):96–108.
13. Petrucci G, Zuccarello B. Fatigue life prediction under wide-band random loading. *Fatigue and Fracture of Engineering Materials and Structures* 2004; **27**(12):1183–1195.
14. Tovo R. Cycle distribution and fatigue damage under broad-band random loading. *International Journal of Fatigue* 2002; **24**(11):1137–1147.
15. Tunna JM. Fatigue life prediction for Gaussian random loads at the design stage. *Fatigue and Fracture of Engineering Materials and Structures* 1986; **9**(3):169–184.
16. Zhao W, Baker MJ. On the probability density function of raiflow stress range for stationary Gaussian processes. *International Journal of Fatigue* 1992; **14**(2):121–135.
17. Kalman RE, Bucy RS. New results in linear filtering and prediction theory. *Journal of Basic Engineering Transactions on ASME*, *Series D* 1961; **83**(3):95–108.
18. Preumont A, Piefort V. Predicting random high cycle fatigue life with finite elements. *ASME Journal of Vibration and Acoustics* 1994; **16**:245–248.
19. You BR, Lee SB. A critical review on multiaxial fatigue assessments of metals. *International Journal of Fatigue* 1996; **18**(4):235–244.
20. Pitoiset X, Preumont A. Spectral methods for multiaxial random fatigue analysis of metallic structures. *International Journal of Fatigue* 2000; **22**:541–550.
21. Sarkani S, Kihl DP, Beach JE. Fatigue of welded joints under narrowband non-Gaussian loadings. *Probabilistic Engineering Mechanics* 1994; **9**:179–190.
22. Wang X, Sun JQ. Multi-stage regression fatigue analysis of non-Gaussian stress processes. *Journal of Sound and Vibration* 2005; **280**:455–465.
23. Sobczyk K, Spencer Jr BF. *Random Fatigue*: *From Data to Theory*. Academic Press: New York, 1992.
24. Spencer Jr BF, Tang J, Artley ME. Stochastic approach to modeling fatigue crack growth. *AIAA Journal* 1989; **27**(11):1628–1635.
25. Casciati F, Colombi P, Faravelli L. Fatigue crack size probability distribution via a filter technique. *Fatigue and Fracture of Engineering Materials and Structures* 1992; **15**(5):463–475.
26. Sobczyk K, Perros K, Papadimitriou C. Fatigue reliability of multidimensional vibratory degrading systems under random loading. *ASCE Journal of Engineering Mechanics* 2010; **136**(2):179–188.
27. Bishop NNM, Sherrat F. A theoretical solution for the estimation of the rainflow ranges from power spectral density data. *Fatigue and Fracture of Engineering Materials and Structures* 1990; **13**(4):311–326.
28. Benasciutti D, Tovo R. Spectral methods for lifetime prediction under wide-band stationary random processes. *International Journal of Fatigue* 2005; **27**:867–877.
29. Franklin GF, Powell JD, Workman ML. *Digital Control of Dynamic Systems* (2nd edn). Addison-Wesley: Reading, MA, 1990.
30. Stengel RF. *Stochastic Optimal Control*: *Theory and Applications*. John Wiley & Son: New York, 1986.
31. Welch PD. The use of fast Fourier transform for the estimation of power spectra: a method based on time averaging over short, modified periodograms. *IEEE Transactions on Audio Electroacoustics* 1967; **AU-15**:70–73.
32. Hayes M. *Statistical Digital Signal Processing and Modeling*. Wiley: New York, 1996.
33. Papadimitriou C. Optimal sensor placement methodology for parametric identification of structural systems. *Journal of Sound and Vibration* 2004; **278**(4):923–947.

DOI: 10.1002/stc